Laminate Design for a Tapered FRP Structure with Ply Drop-off Based on Yielding of Resin Pockets

Sae Obata[a], Kosuke Takahashi[b,*], Kazuaki Inaba[a]

[a] *Graduate Major in Mechanical Engineering, School of Engineering, Tokyo Institute of Technology, 2-12-1 Ookayama, Meguro, Tokyo 152-8552, Japan*

[b] *Division of Mechanical and Space Engineering, Hokkaido University, N13, W8, Kita-ku, Sapporo, Hokkaido 060-8628, Japan*

ABSTRACT

In this study, a design procedure is proposed for a tapered FRP laminate with ply drop-offs to suppress the damage initiation. A stress index, based on the von Mises yield criteria, is defined and applied to the resin pockets formed adjacent to cut plies. First, finite element (FE) analysis of a three-ply tapered laminate consisting of a cover layer, a dropped layer, and a base layer is conducted to relate the fiber directions with the stresses caused by a ply drop-off. Using the stress values obtained from the FE analysis, a tapered quasi-isotropic laminate with a

* Corresponding Author. *E-mail address*: ktakahashi@eng.hokudai.ac.jp

Abbreviations. FRP: fiber-reinforced plastic; SEM: scanning electron microscopy.

thickness decreasing from 16 to 8 layers is appropriately designed by minimizing the overall stress indexes in ply-dropped locations. The observation of the specimen manufactured by autoclave molding reveals that the resin pockets can be effectively eliminated by the appropriate design. The tensile tests also verify the higher load capacity.

Keywords: A. Carbon fibre, B. Strength, D. Mechanical testing, Ply drop-off

1. Introduction

Tapered structures are often prepared from fiber-reinforced polymer (FRP) laminates to improve their aerodynamic characteristics and reduce weights. However, such structures are not manufactured by machining methods, which are widely utilized for metal structures, to prevent their fibers surrounded by a resin matrix from being exposed; otherwise, exposed fibers would initiate damage and decrease the material strength considerably [1,2]. Instead, the thickness distribution of the structure is usually implemented by cutting plies inside laminates, called ply drop-offs, to avoid machining the outer plies and keep the resin layer for covering the structural surface. However, the discontinuity of cut plies would still initiate various damages such as delamination and matrix cracking because of the stress concentration [3–11]. The stacking sequences and fiber directions of the discontinued layers are strongly related to its strength when multiple plies are dropped in a laminate structure. It is desirable to suppress these damages by locating cut plies effectively, but difficult since the initiation of the

damage depends on various factors such as the taper angle, offset of the ply drop, and locations of dropped plies [7,12]. Consequently, the design of tapered laminates with ply drop-offs requires to consider diverse lamination configuration parameters such as stacking sequences, fiber directions of dropped plies, and end thickness [13]. Therefore, the applications of tapered FRP structures are limited to the extremely conservative designs constrained by sufficiently small taper angles.

As of today, several design guidelines have been proposed to prevent strength losses due to ply cutting in tapered laminates [14-21]:

- Minimize the number of discontinued layers at each location
- Keep the distance between the dropped layers at least three times with respect to ply thickness
- Cut the 0° layer first and the 90° layer last
- Maintain the structural symmetry
- Cut the inner layer first
- Do not cut the 0° and 90° layers adjacent to each other.

However, these guidelines are only qualitative, and the appropriate laminate patterns cannot be derived automatically. Therefore, it is desirable to establish design guidelines, which can quantitatively determine the optimized laminate pattern of high-strength tapered laminates while considering the layout of discontinuous layers. For this purpose, it is necessary to develop a design index, based on which the stacking pattern of a tapered laminate can be optimized to suppress the degradation of its strength. Various failure criteria have been applied to predict the strengths of tapered laminates [22]. Curry et al. [6] utilized the interlaminar fracture criteria based on the mixed failure mode [23]. Fish et al. [13] investigated the delamination based on the Tsai-wu criterion

[24]. These interlaminar fractures were initiated from the failure at the resin-rich areas around the dropped layer [25]. Vizzini [12,26] examined the delamination origins at the resin-rich layer between different layers and estimated their von Mises stress values. The delamination near discontinuous layers was also found to be closely related to the yielding of resin pockets by Nakatani et al.[27]. Crack initiation inside the resin pocket of a tapered structure was observed by Vizzini and Lee [4], who also concluded that the resin pocket had yielded prior to delamination using an analytical model. These findings suggest that the yielding of resin pockets due to ply discontinuities seems a suitable failure criterion for the optimal design of a tapered laminate.

In this study, a stress index, based on the von Mises yield criteria, is defined and applied to the resin pockets adjacent to discontinuous layers to establish a quantitative design guideline for a tapered FRP laminate with ply drop-off. Stress analysis is conducted using a three-dimensional finite element model, consisting three plies including single cut ply and a resin pocket, for obtaining the stress index in the resin pocket for various stacking patterns. The tapered laminate is then appropriately designed using the proposed stress index. Tensile tests are finally conducted using the designed tapered laminate to verify the effectiveness of the proposed stress index.

2. Design of stacking patterns based on the yielding of resin pockets

2.1. Stress analysis of a resin pocket by a three-ply finite element model

A finite element (FE) model of the tapered laminate consisting of three plies was constructed as shown in Fig. 1, to relate stresses within a resin pocket with fiber directions of plies under a tensile loading. For these plies, denoted by a cover layer, a dropped layer, and a base layer from top to bottom, all possible stacking patterns of

fiber directions represented by 0°, ±45°, and 90° angles were considered. The finite element analysis was conducted by Abaqus/CAE 2017 software. The thickness of each layer in Fig. 1 was set to 0.2 mm, and the taper slope (the ratio expressed as thickness reduction / longitudinal length), at which its magnitude decreased from the thickness of three layers to that of two layers, was set to 1/5. The taper slope was adjusted to the tapered laminates manufactured by autoclave molding for the tensile test in section 3.1. The face of the left edge of the model was fixed, and a displacement of 0.009 mm (0.1% of the average strain across the entire model length) was applied to the face of the right edge in the *x*-direction to express the uniaxial loading. The material properties based on the properties of prepreg (PYROFIL #380, Mitsubishi Rayon Co. Ltd) are listed in Table 1. Here, subscript 1 represents the fiber direction, and subscripts 2 and 3 denote the directions perpendicular to the fiber direction. The triangular area surrounded by the three plies in Fig. 1 was modeled as a resin pocket filled exclusively with epoxy resin; therefore, its properties were identical of those of the resin. The elements inside the resin pocket used a quadratic tetrahedral element (C3D8R) with 22,792 elements and those in three layers used linear hexahedral elements (C3D10) with 80,000 elements with a total number of nodes equal to 126,694.

The representative stress values in the resin pocket were taken from the element located at the center of gravity (the red point in Fig. 1) because those used for the design of tapered laminates should not be excessively affected by the stress concentration at the specific corner of the resin pocket. The stress concentration is not always the most significant at the sharpest corner of the triangle, but also at the other corners depending on the stacking patterns. In addition, the stress values on the element located at the corner is sensitive to the meshing and the shape of the resin pocket, which also varies

for each stacking pattern. Even if all possible patterns of three plies are examined for modeling the actual shape of the resin pocket in advance, they may differ from those formed in the thick tapered laminate with multiple cut plies. Therefore, stress values at the center of gravity in the fixed triangle of resin pocket are regarded to be more suitable for comprehensively evaluating the stress concentration at all corners with the effects of the fiber directions and practical for the design of tapered laminates.

Table 2 lists the von Mises stresses at the center of gravity of the resin pocket computed for each stacking pattern. In this table, the fiber directions of the cover layer and base layer are provided in the upper row, and the fiber directions of the dropped layer are listed in the left column. A total of 36 different patterns are obtained. Here, the layer of fiber angle 45° and -45° are considered to be the same pattern because there is no difference of von Mises stress (for example, the lamination configurations [+45/90/–45] and [–45/90/+45]). The values of Mises stresses less than 5 MPa are colored dark blue; those greater than 5 and less than 10 are colored light blue; those greater than 10 and less than 15 are colored orange; and those greater than 15 are colored red. When the fiber angle of the cover layer is equal to 90°, the stress values in most cases are less than 5 MPa except for the case when the fiber angle of the dropped layer is 0°. When the fiber angle of the cover layer is 0°, the stress values exceed 10 MPa and are higher than most of the other values listed in the table regardless of the fiber orientation of the dropped layer. In case of the same cover layer / base layer combinations, the highest magnitudes correspond to the fiber angle of the dropped layer equal to 0°. For the same combination of the base layer and cover layer (such as 0/90 and 90/0), their swapping at the same fiber angle of the dropped layer significantly affects the stress value. Once the preferable patterns of the cover, dropped, and base layers are clarified by the data

presented in this table, a stacking pattern of the target tapered structures based on these patterns can be designed to minimize the influence of ply-dropped regions [28].

2.2. Stress index equation

Using the stress values calculated by the three-ply model, a stress index that indicates an initiation of failure at the resin pocket is defined. It is necessary to consider the thickness at each resin pocket N and the thickness of the thick section N_0 for the laminate with multiple resin pockets, as depicted in Fig. 2. Since the increase of the tensile stress in the longitudinal direction due to the thickness decrease is expressed by the factor of N_0/N, the stress index σ'_{M} to design a tapered laminate with multiple cut plies can be computed via equation (1).

$$\sigma'_{\mathrm{M}} = \frac{1}{\mathrm{E}\varepsilon}\left[\frac{1}{2}\left\{\left(\frac{N_0}{N}\sigma_{xx} - \sigma_{yy}\right)^2 + \left(\sigma_{yy} - \sigma_{zz}\right)^2 + \left(\sigma_{zz} - \frac{N_0}{N}\sigma_{xx}\right)^2 + 6\left(\tau_{xy}^2 + \tau_{yz}^2 + \tau_{zx}^2\right)\right\}\right]^{\frac{1}{2}} \quad (1)$$

It is normalized by the average strain computed across the longitudinal length of the entire model (ε) and Young's modulus of the resin pocket (E) to make it independent of the displacement applied to the finite element model. Each stress component calculated at the center of gravity of the resin pocket through the three-layer analysis conducted in section 2.1 is used for obtaining the stress index of equation (1) and designing the appropriate pattern of tapered laminates.

2.3. Laminated pattern design

Using the stress index defined in section 2.2, laminates with multiple cut plies were designed. In particular, a tapered quasi-isotropic laminate [+45/–45/90/0/+ 45/–

$45/90/0]_n$ with a number of layers decreasing from 16 (n = 2) to 8 (n =1) was examined by cutting eight plies to maintain the quasi-isotropic laminate configuration in both the thick and thin sections. Because the surface layer of aircraft components generally has a ±45° configuration [29], the upper and lower ±45° layers were fixed as continuous layers, and the remaining 12 layers were considered to be potential cut plies. Resin pockets were arranged sequentially inside the tapered section that was divided into eight segments along the longitudinal direction. In addition, none of these pockets were placed in adjacent positions because such a layout would decrease the material strength significantly due to the superposition of stress concentration.

Under these conditions, the appropriate stacking pattern can be derived by minimizing the stress index at all the locations of cut plies. There are several approaches by focusing on either the highest stress index among all, the average stress index, or the stress index at thinner section. In this study, the priority was given to realize the lower stress index at the thinner section with low overall stress indexes, and the appropriate pattern was derived as shown in Fig. 3(a). A reference pattern which includes high value stress indexes was also obtained for comparison as shown in Fig. 3(b). The ply drop-off locations in the thick sections are denoted A1, A2, …, A8 (appropriate pattern) and R1, R2, …, R8 (reference pattern), and the value of the stress index σ'_{M} calculated for each location is shown in Fig. 4. It was confirmed that the stress index of the appropriate pattern (Fig. 4(a)) was lower than the stress index of the reference pattern (Fig. 4(b)). In addition, its highest values were obtained for locations A3 (appropriate pattern) and R7 (reference pattern). Therefore, when tensile load is applied to these laminated patterns, the initial damage is expected to occur in resin pockets A3 and R7, but delayed for the appropriate pattern, which results in the higher load capability.

3. Experimental validation of the proposed design guidelines

3.1. Manufacturing laminates with ply drop-offs

Specimens with the laminated pattern described in Figs. 3(a) and (b) were manufactured using unidirectional prepreg (PYROFIL TR 380G250S, Mitsubishi Rayon) by autoclave (DANDELION, Hanyuda Ironworks) molding. The curing conditions is specified in Table 3. In the laminate plate with a size of 140 × 190 mm, the tapered section was located in the middle along the longitudinal direction. The aspect ratio of the tapered section (thickness reduction/ longitudinal length) was set to 1/5, which was designed to fall within the range of the taper angle 7 to 27 degrees [21]. The laminate was cut with a diamond cutter to form the specimen depicted in Fig. 5.

Shapes of the resin pockets were observed from the side surface after careful polishing under a three-dimensional microscope VE-8800 (Keyence) operated in the secondary electron detection mode at an acceleration voltage of 1.0 kV. Because the resin pockets and fibers are shown as dark grey and light grey objects, respectively, the discontinued layers can be easily found in the obtained images. Figs. 6 and 7 show the scanning electron microscopy (SEM) images of the areas around resin pockets A1–A8 of the appropriate pattern and R1–R8 of the reference pattern, respectively. In the appropriate pattern, resin pockets with triangle shapes were not observed because the fibers of the cover and base layers flowed into the locations of cut plies, whereas they were clearly formed at the R2, R3, R4, R5, and R8 locations of the reference pattern. When 90° layers were laminated on either the cover or the base layer at the A1, A2, A3, A4, A8, R1, R6, and R7 locations, the fibers can easily move to fill the region next to cut plies. At the A5 and A6 locations, where the cut ply was sandwiched by 90° layers,

the fibers flowed from both the cover and base layers . When the cover and base layers did not include 90° (such as those at the R2, R3, R4, R5 and R8 locations), the ply-dropped region was hardly filled with the fibers and resulted in forming the triangular resin-rich regions, which would cause the initiation of failures. Therefore, it was confirmed that designing the stacking pattern of tapered laminates by the proposed stress index can successfully eliminate the cause of the significant stress concentration at the ply-dropped region.

3.2. Tensile testing

A tensile test using the tapered specimen fabricated in section 3.1 was performed on an INSTRON 5982 universal testing machine at a tensile speed of 5.0 mm/min, as shown in Fig. 8. Six laminate specimens were prepared for both the appropriate and reference patterns. Five of these specimens were subjected to a monotonic tensile load until fracture. The remaining specimen was subjected to gradual tensile load stepwise at a displacement of approximately 1 mm and then held for a while to take images of the tapered section for detail observation of damage progress. After the careful examination of damage monitoring, further displacement was applied manually at a 0.1 mm increment. These procedures were repeated until significant damage was observed. Damage initiation and propagation may be clearly detected during a tensile test because the 0° layer can be clearly identified under a digital microscope. In each test, a pretension of 0.50 kN was applied to the specimen to avoid variations of the clamping conditions.

3.3. Results and discussion

Fig. 9 shows the results of the tensile test obtained for the appropriate and reference patterns, denoted by the blue and red lines, respectively. Here, the applied load is divided by the specimen width to avoid effects caused by its slight variations. The solid lines in the plots represent the load-displacement curves recorded under monotonic loading until fracture, and the markers denote the loads applied at every 0.1 mm increment for the careful damage observation. The results indicate that the load slightly decreased at approximately 0.7 kN/mm for the appropriate pattern and at 0.6 kN/mm for the reference pattern. In addition, the greater decrease of load was observed for the reference pattern. The load decreased again at 1.0 kN/mm for the appropriate pattern, but increased again up to 1.1 kN/mm. On the other hand, the reference pattern caused fracture at the displacement of 2.9 mm, where the second decrease of load was observed for the appropriate pattern. Fig. 10 displays the load when the initial decrease was observed and the final maximum load when the specimen fractured. They were averaged from the five specimens. These results verify that the appropriate pattern is more durable than the reference pattern.

The microscopic image of the entire tapered section obtained for the appropriate pattern was observed as shown in Fig. 11(a). The areas of blue and green windows are magnified in the following images of Figs. 11(b)–(f). Fig. 11(b) was taken before loading, and Fig. 11(c)-(f) were taken at the corresponding points (c)-(f) in Fig. 9. At a load of 0.44 kN/mm (Fig. 11(c)), a small crack was observed in the vicinity of the lower 0° layer along the vertical direction. At a load of 0.53 kN/mm (Fig. 11(d)), a small crack propagated from the center of the 0° layer near the thin section, as shown in the green window. When the load reached 0.60 kN/mm (Fig. 11(e)), a relatively large crack occurred and caused the initial load decrease. After the load exceeded 0.67 kN/mm (Fig.

11(f)), this crack propagated to the specimen end through delamination, leading to the formation of multiple small cracks. Fig. 12 shows the images of the damage propagation obtained for the reference pattern. The entire tapered section is shown in Fig. 12(a). The red, orange, and yellow windows of Fig 12 (b)–(f) are the magnified images of the corresponding squares in Fig. 12(a). No damage was confirmed before loading as shown in in Fig. 12(b). At a load of 0.41 kN/mm (Fig. 12(c)), crack initiation was observed near the dropped region of the lower 0° layer. At a load of 0.50 kN/mm (Fig. 12(d)), another small crack occurred vertically across the middle 0° layer. When the load reached 0.61 kN/mm (Fig. 12(e)), the initial crack generated near the dropped region of the lower 0° layer propagated drastically, as shown in Fig. 12(f), and caused a significant load decrease.

These observations revealed that initial cracks were formed in the lower 0° layers of both the appropriate and reference patterns. The locations of damage initiation corresponded well to the ply-dropped locations of the highest stress indexes depicted in Fig. 3 (A3 and R7). In the laminate specimen with the reference pattern, the initial crack propagated and caused the initial decrease of load. Meanwhile, the initial crack detected in the laminated specimen with the appropriate pattern did not propagate further, but the other subsequent crack propagated to cause the initial load decrease. These results indicate that the proposed stress index is an effective index for designing tapered laminates with ply drop-offs, but its magnitude has not been optimized yet. Although the stress index was calculated in the framework of the three-ply finite element model, the loading conditions for the thick tapered laminate with multiple cut plies would be slightly different because the base layer is not always parallel to the bottom surface, but may be inclined. The influence of bending deformation should be also taken into

account due to the offset of the thin section. Hence, the simple approach proposed in this study can be further improved by conducting a more detailed stress analysis and optimizing the stacking pattern to minimize the stress index more effectively.

4. Conclusion

In this study, new design index was proposed for the tapered structures with ply drop-offs. First, stress analysis for a resin pocket formed in a three-ply tapered laminate was conducted by a finite element method. Using the stress values obtained from the stress analysis, the corresponding stress index was calculated to design the tapered quasi-isotropic laminate with a thickness decreasing from 16 layers to 8 layers. Two laminates, one by appropriate pattern and the other by reference pattern, were designed and manufactured by autoclave molding. The observation under SEM revealed that the resin pockets adjacent to the cut plies were effectively eliminated by stacking 90° layers for the appropriate pattern, but formed with the clear triangular shapes for the reference pattern. Finally, tensile testing was conducted under a careful observation of the tapered section to monitor damage initiation and progress. It was confirmed that the specimen for the appropriate pattern exhibited higher strength. In addition, an initial crack was detected near the discontinued region of the lower 0° layer, which corresponded well to the location of the highest stress index.

Acknowledgments

This work was supported by Council for Science, Technology and Innovation(CSTI), Cross-ministerial Strategic Innovation Promotion Program (SIP), “Structural Materials for Innovation” (Funding agency:JST).

References

1. Hosoi A, Arao Y, Kawada H. Transverse crack growth behavior considering free-edge effect in quasi-isotropic CFRP laminates under high-cycle fatigue loading. Compos Sci Technol 2009;69(9):1388-1393.
2. Yokozeki T, Aoki T, Ishikawa T. Fatigue growth of matrix cracks in the transverse direction of CFRP laminates. Compos Sci Technol 2002;62(9):1223-1229.
3. Abdulhamid H, Bouvet C, Michel L, Aboissière J, Minot C. Influence of internally dropped-off plies on the impact damage of asymmetrically tapered laminated CFRP. Compos A Appl Sci Manuf 2015;68:110–120.
4. Vizzini AJ, Lee SW. Damage analysis of composite tapered beams. J Am Helicopter Soc 1995;40(2):43–49.
5. Llanos AS, Vizzini AJ. The effect of film adhesive on the delamination strength of tapered composites. J Compos Mater 1992;26(13):1968–1983.
6. Curry JM, Johnson ER, Starnes JH. Effect of dropped plies on the strength of graphite-epoxy laminates. AIAA J 1992;30(2):449–456.
7. Murri GB, Schaff JR. Fatigue life methodology for tapered hybrid composite flexbeams. Compos Sci Technol 2006;66(3–4):499–508.
8. Xing YM, Yun H, Dai FL. An experimental study of failure mechanisms in laminates with dropped plies. Compos Sci Technol 1999;59(10):1527–1531.
9. Wisnom MR, Jones MI, Cui W. Failure of tapered composites under static and fatigue tension loading. AIAA J 1995;33(5):911–918.

10. Weiss A, Trabelsi W, Michel L, Barrau JJ, Mahdi S. Influence of ply-drop location on the fatigue behaviour of tapered composites laminates. Procedia Eng 2010;2(1):1105–1114.

11. Steeves CA, Fleck NA. Compressive strength of composite laminates with terminated internal plies. Compos A Appl Sci Manuf 2005;36(6):798–805.

12. Vizzini AJ. Influence of realistic ply-drop geometries on interlaminar stresses in tapered laminates. In: Martin R, editor. Composite Materials: Fatigue and Fracture: Fifth Volume. West Conshohocken, PA: ASTM International, 1995, p. 467–485.

13. Fish JC, Lee SW. Delamination of tapered composite structures. Eng Fract Mech 1989;34(1):43–54.

14. Cairns DS, Mandell JF, Scott ME, Maccagnano JZ. Design and manufacturing considerations for ply drops in composite structures. Compos B Eng 1999;30(5):523–534.

15. Peeters D, Abdalla M. Optimization of ply drop locations in variable-stiffness composites. AIAA J 2016;54(5):1760–1768.

16. Paul PC, Saff CR, Sanger KB, Mahler MA, Kan HP, Kautz EF. Out of plane analysis for composite structures. NASA Tech Rep 1990;263–279.

17. Mukherjee AB, Varughese B. Design guidelines for ply drop-off in laminated composite structures. Compos B Eng 2001;32(2):153–164.

18. Adams DB, Watson LT, Gürdal Z, Anderson-Cook CM. Genetic algorithm optimization and blending of composite laminates by locally reducing laminate thickness. Adv Eng Softw 2004;35(1):35–43.

19. Irisarri FX, Lasseigne A, Leroy FH, Le Riche R. Optimal design of laminated composite structures with ply drops using stacking sequence tables. Compos Struct 2014;107:559–569.

20. Allegri G, Kawashita LF, Backhouse R, Wisnom MR, Hallett SR. On the optimization of tapered composite laminates in preliminary structural design. In: Proceedings of ICCM-17 Conference. Edinburgh, July, 2009, p. 27–31.

21. Gan KW, Allegri G, Hallett SR. A simplified layered beam approach for predicting ply drop delamination in thick composite laminates. Mater Des 2016;108(15):570–580.

22. He K, Hoa SV, Ganesan R. The study of tapered laminated composite structures: A review. Compos Sci Technol 2000;60(14):2643–2657.

23. Hashin Z. Failure criteria for unidirectional fiber composites. J Appl Mech Trans 1980;47(2):329–334.

24. Tsai SW, Wu EM. A general theory of strength for anisotropic materials. J Compos Mater 1971;5(1):58–80.

25. Kemp BL, Johnson ER. Response and failure analysis of a graphite-epoxy laminate containing terminating internal plies. In: Proceedings of the AIAA/ASME/ASCE/AHS 26th Structures, Structural Dynamics, and Materials Conference. New York, April, 1985, p. 13–24.

26. Vizzini AJ. Strength of laminated composites with internal discontinuities parallel to the applied load. AIAA J 1992;30(6):1515–1520.

27. Nakatani H, Nakaya K, Matsuba A, Kouno Y, Ogihara S. Damage behavior in unidirectional CFRP laminates with fiber discontinuity. Trans JSME A 2013;79(799):294–303 (in Japanese).

28. Kamo S, Takagi K, Shitani T, Abe T, Obata S, Takahashi K. Method of designing composite material, method of evaluating composite material, and composite material. U.S. Patent No. 16/059,207 (2019).

29. Dutton S, Kelly D, Baker A. Composite Materials for Aircraft Structures, Second Edition. American Institute of Aeronautics and Astronautics, 2004.

Figure captions

Fig. 1. A three-ply finite element model.

Fig. 2. Proposed parameters N, and N_0 for stress analysis performed at various laminate thicknesses.

Fig. 3. (a) Appropriate and (b) reference laminated patterns.

Fig. 4. Stress indexes calculated at various ply drop-off locations of the (a) appropriate and (b) reference patterns.

Fig. 5. Geometry of the tapered laminate specimen for tensile testing.

Fig. 6. SEM images of the regions around the resin pockets in the appropriate pattern.

Fig. 7. SEM images of the regions around the resin pockets in the reference pattern.

Fig. 8. An experimental setup for a tensile test.

Fig. 9. Load – displacement curves recorded during the monotonic/stepwise tensile test.

Fig. 10. Load at damage initiation and final fracture for the appropriate and reference patterns.

Fig. 11. Images of the tapered laminate specimen with the appropriate pattern. (a) An overview of the tapered area. The colored squares show the images of the corresponding regions in panel (a) obtained (b) before loading, (c) at a displacement of 1.0 mm and load of 0.44 kN/mm, (d) at a displacement of 1.3 mm and load of 0.53 kN/mm, (e) at a displacement of 1.5 mm and load of 0.60 kN/mm, and (f) at a displacement of 1.8 mm and load of 0.67 kN/mm.

Fig. 12. Images of the reference pattern. (a) An overview of the tapered area. The colored squares show the image of the corresponding regions in panel (a) obtained (b) before loading, (c) at a displacement of 0.9 mm and load of 0.41 kN/mm, (d) at a displacement of 1.2 mm and load of 0.50 kN/mm, (e) at a displacement of 1.5 mm and

load of 0.61 kN/mm, and (f) after the tensile testing machine stopped at a displacement of 1.5 mm.

Tables

Table 1 Mechanical properties for the finite element simulation.

	FRP	Resin (epoxy)
Young's modulus [GPa]	$E_1 = 137$ $E_2 = E_3 = 8.9$	$E_{epoxy} = 3.5$
Shear modulus [GPa]	$G_{12} = G_{13} = 4.0$ $G_{23} = 3.2$	–
Poisson's ratio	$\nu_{12} = \nu_{13} = 0.32$ $\nu_{23} = 0.37$	$\nu_{epoxy} = 0.37$

Table 2 Von Mises stresses calculated at the centers of gravity of the resin pockets.

[MPa]		Cover / base layers									
		0/0	0/45	0/90	45/0	45/45	45/–45	45/90	90/0	90/45	90/90
Dropped layer	0°	14.16	19.03	17.65	8.47	8.56	9.56	10.57	7.06	7.32	6.83
	45°	12.10	14.63	12.02	5.86	5.24	8.04	6.38	4.22	4.41	5.09
	–45°		15.93		5.93	6.13	7.73	7.16		4.99	
	90°	11.86	13.99	12.27	5.63	4.93	7.79	6.59	3.80	4.14	4.52

Table 3 Parameters of the heating and curing procedures.

Parameter	Heating	Curing
Retention temperature [°C]	80	135
Heating rate [°C/min]	2.1	1.8
Holding pressure [MPa]	0.65	0.65
Holding time [min]	60	150

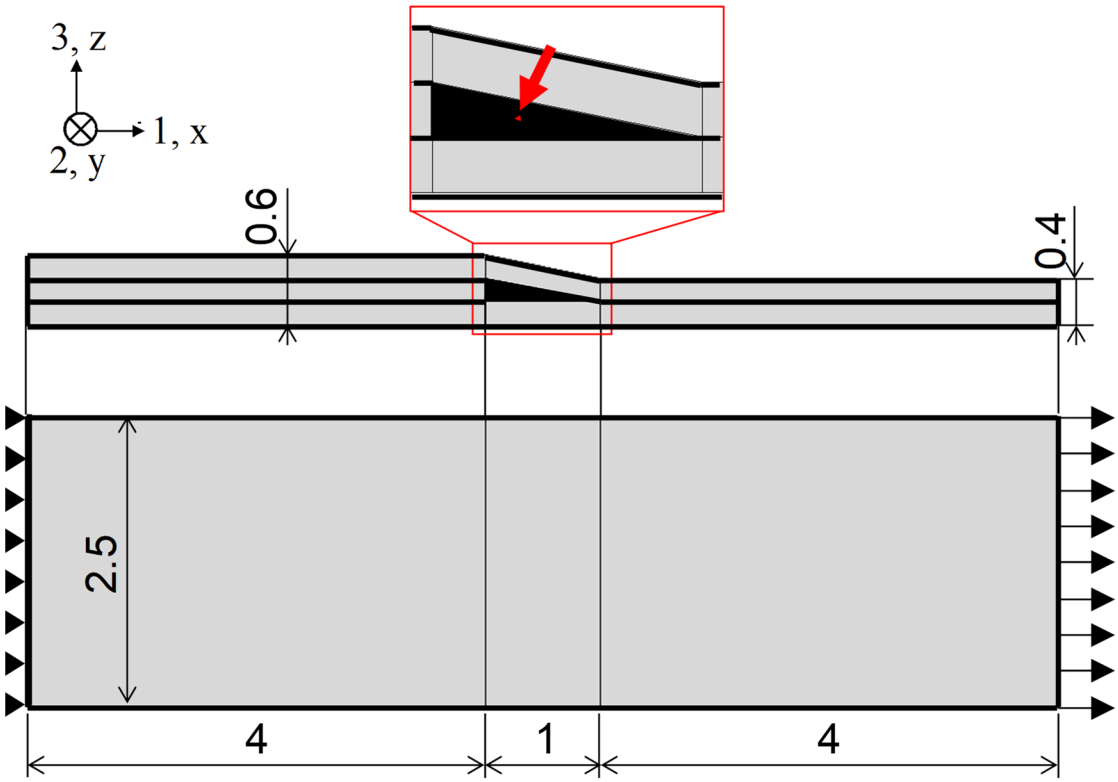

All dimensions are expressed in millimeters

Fig. 1

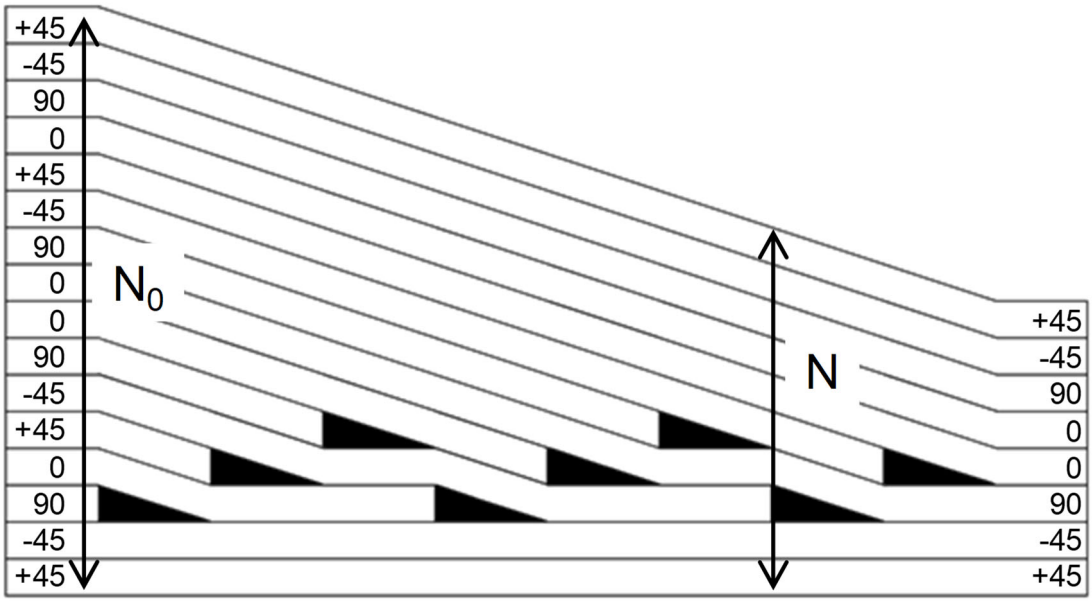

Fig. 2

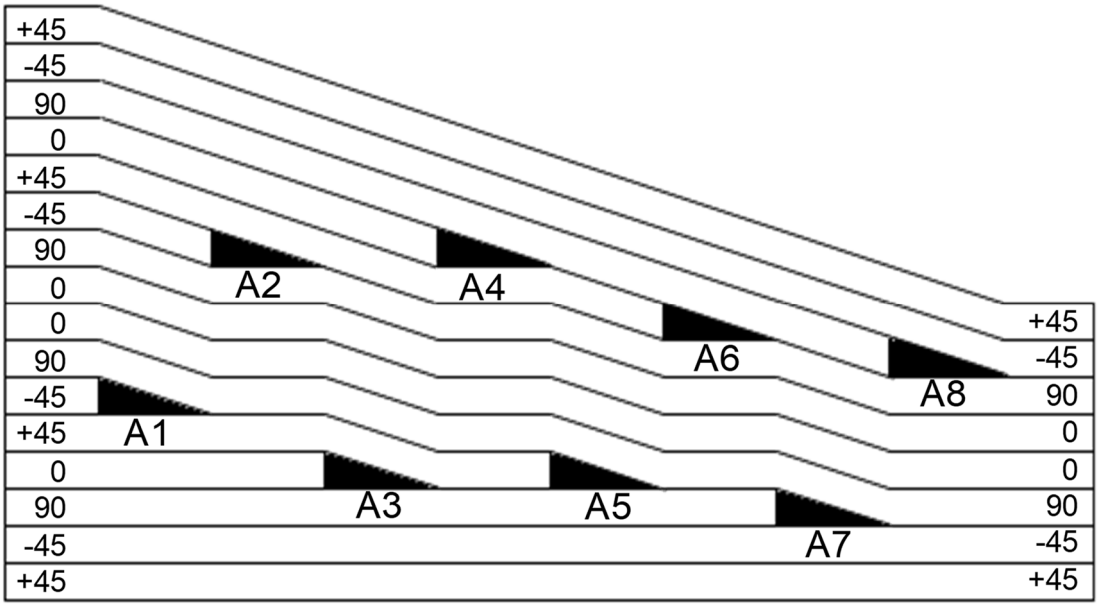
+45
-45
90
0
+45
-45
90
0
0
90
-45
+45
0
90
-45
+45
A1
A2
A3
A4
A5
A6
A7
A8
+45
-45
90
0
0
90
-45
+45

(a)

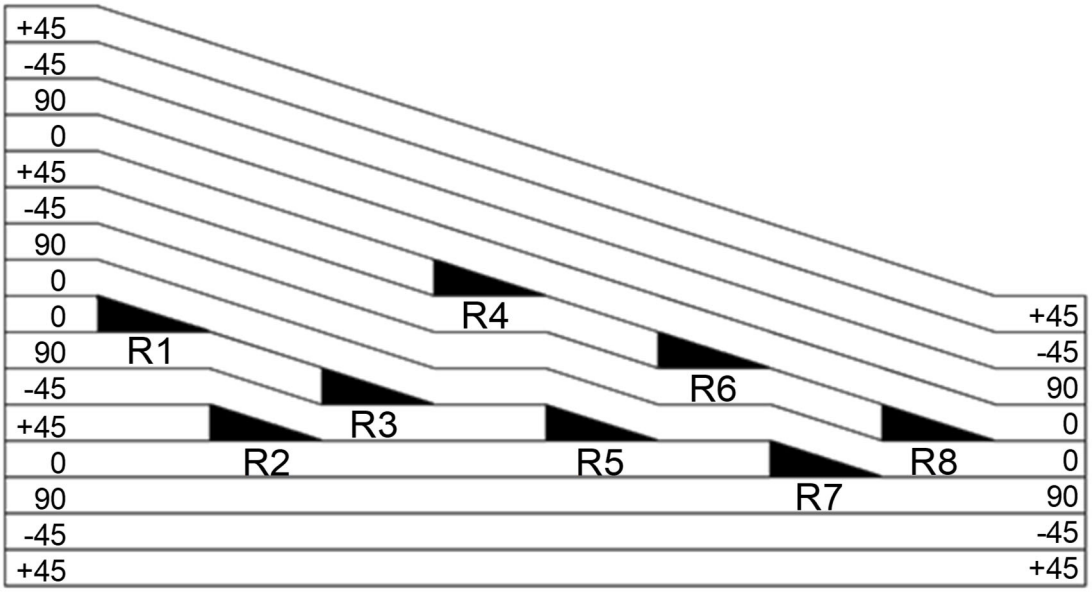
+45
-45
90
0
+45
-45
90
0
0
90
-45
+45
0
90
-45
+45
R1
R2
R3
R4
R5
R6
R7
R8
+45
-45
90
0
0
90
-45
+45

(b)

Fig. 3

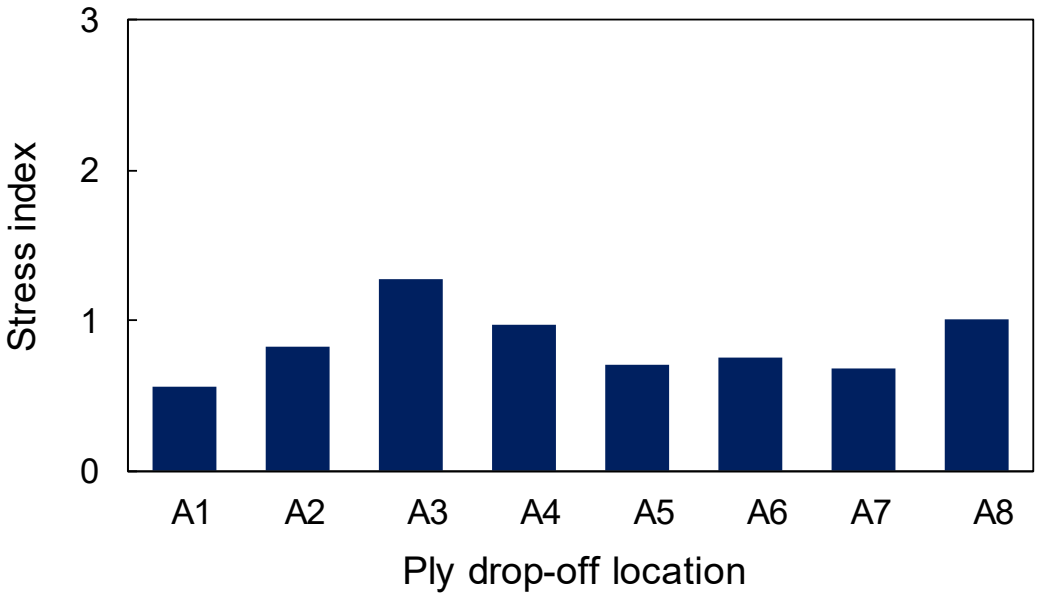
Stress index
3
2
1
0
A1
A2
A3
A4
A5
A6
A7
A8
Ply drop-off location

(a)

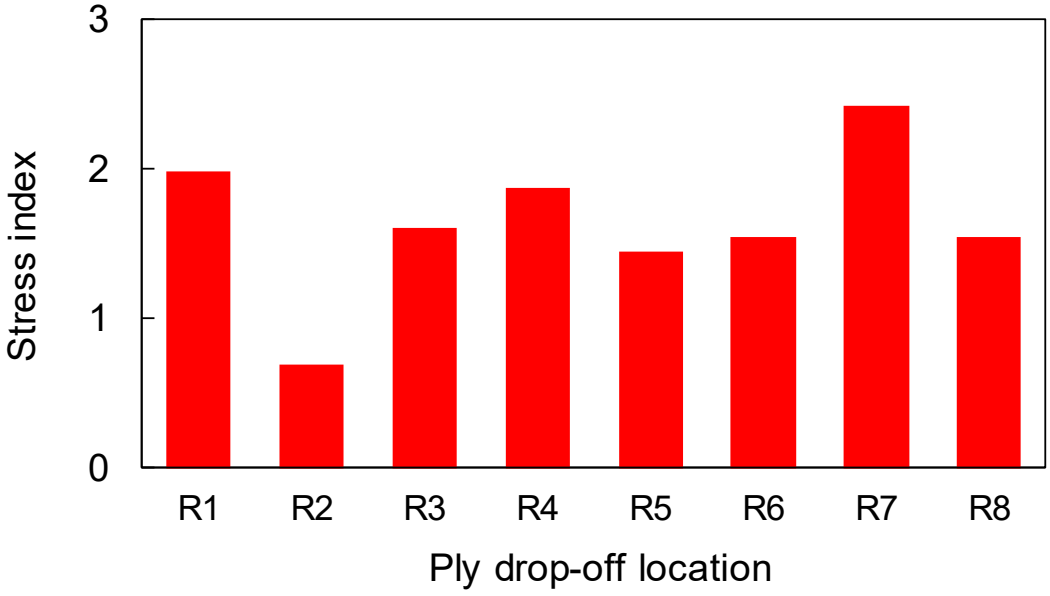
Stress index
3
2
1
0
R1
R2
R3
R4
R5
R6
R7
R8
Ply drop-off location

(b)

Fig. 4

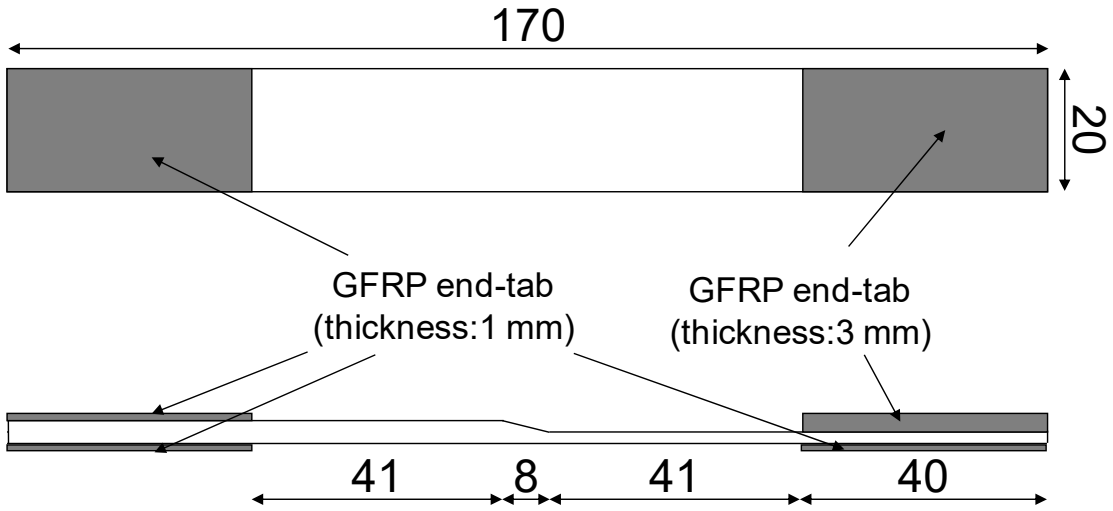
170
20
GFRP end-tab
(thickness:1 mm)
GFRP end-tab
(thickness:3 mm)
41
8
41
40

Fig. 5

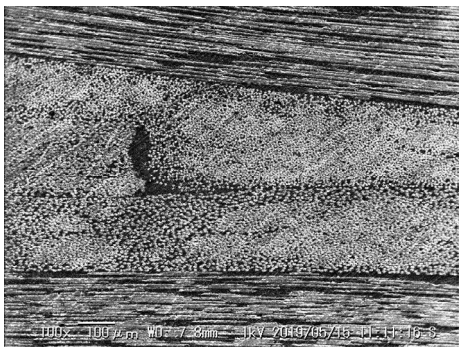

A1 (90/–45/45)

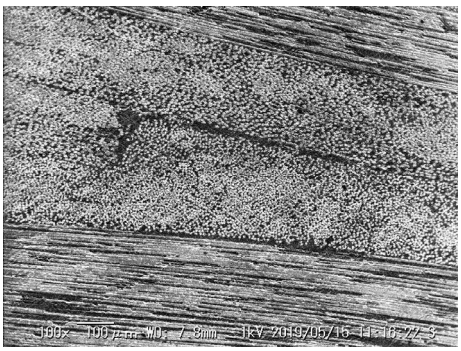

A2 (45/–45/90)

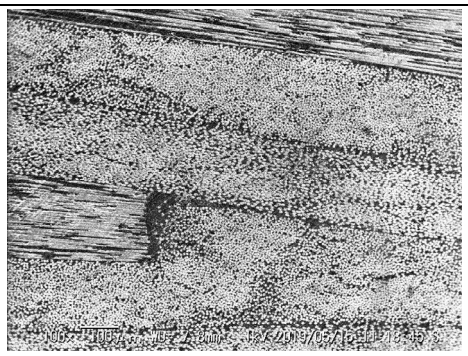

A3 (45/0/90)

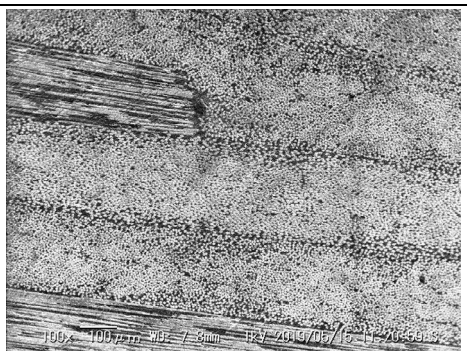

A4 (90/0/45)

A5 (90/45/90)

A6 (90/45/90)

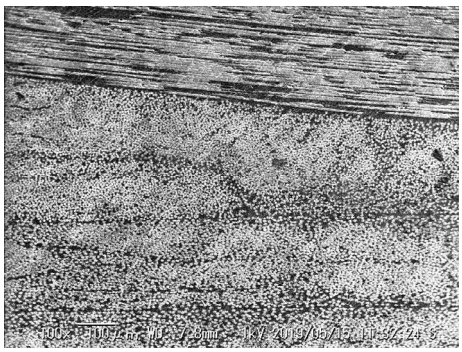

A7 (90/90/–45)

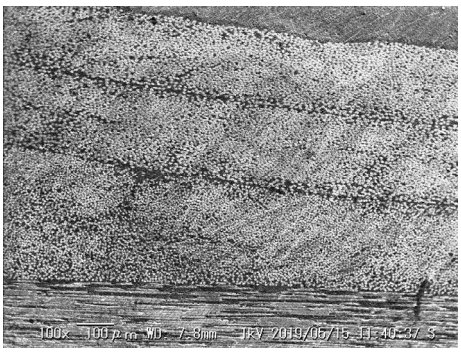

A8 (–45/90/90)

Fig. 6

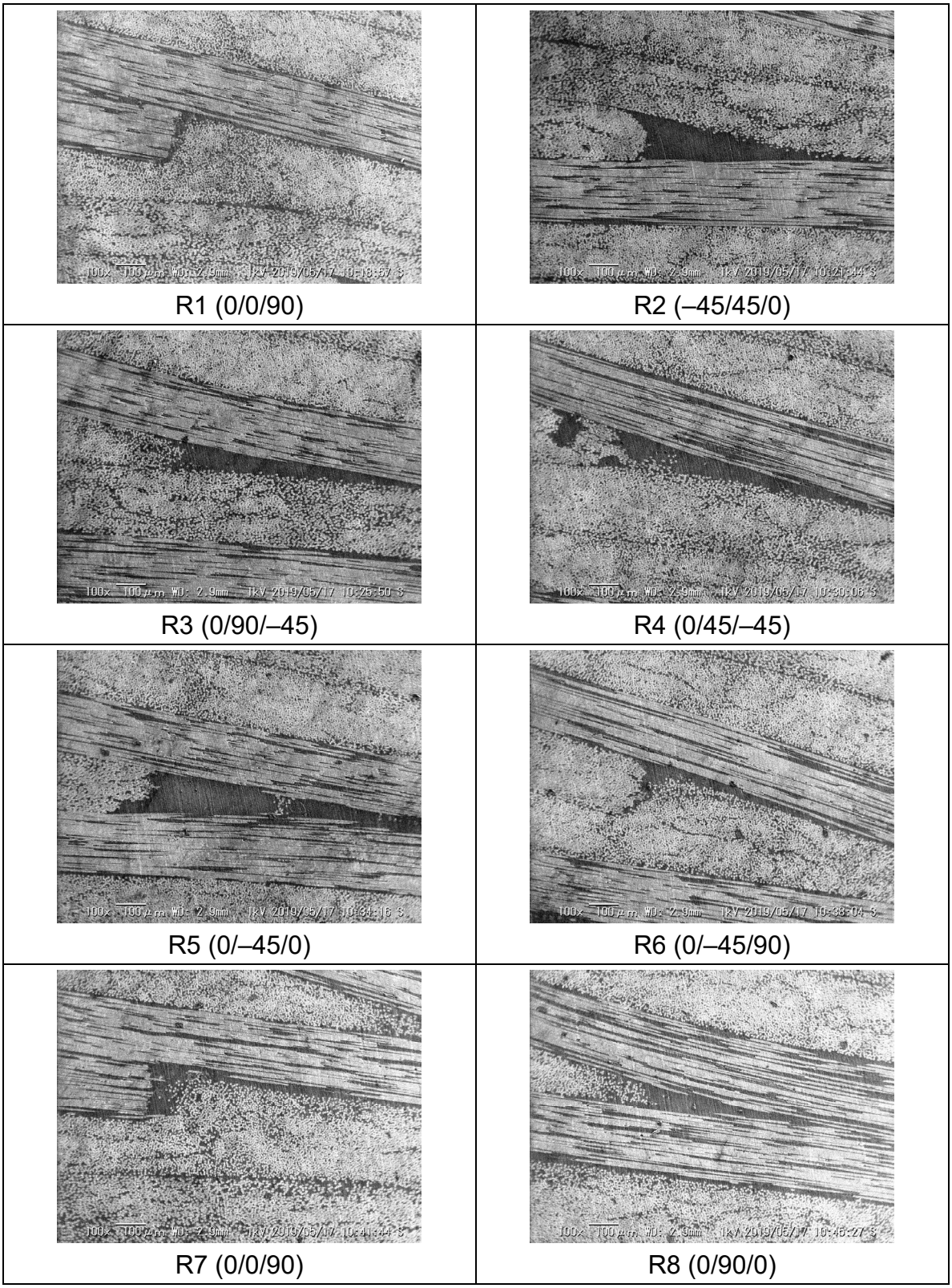
R1 (0/0/90)
R2 (–45/45/0)
R3 (0/90/–45)
R4 (0/45/–45)
R5 (0/–45/0)
R6 (0/–45/90)
R7 (0/0/90)
R8 (0/90/0)

Fig. 7

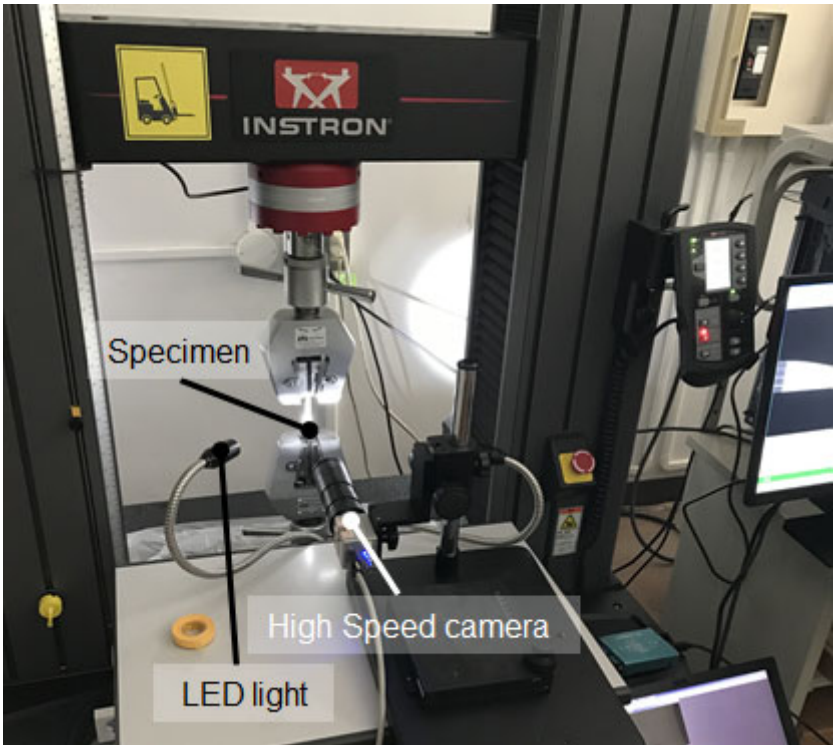

Fig. 8

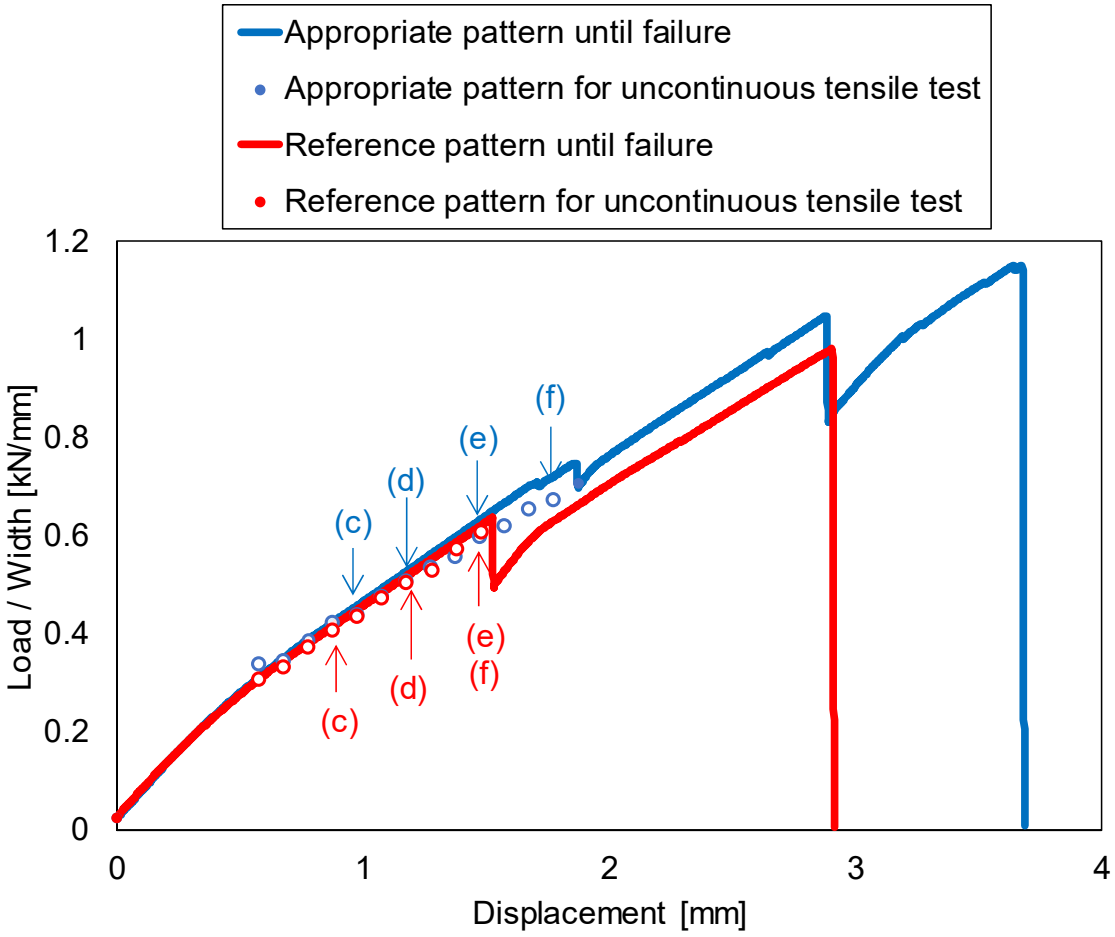
Appropriate pattern until failure
Appropriate pattern for uncontinuous tensile test
Reference pattern until failure
Reference pattern for uncontinuous tensile test
Load / Width [kN/mm]
Displacement [mm]
1.2
1
0.8
0.6
0.4
0.2
0
0
1
2
3
4
(c)
(d)
(e)
(f)
(c)
(d)
(e)
(f)

Fig. 9

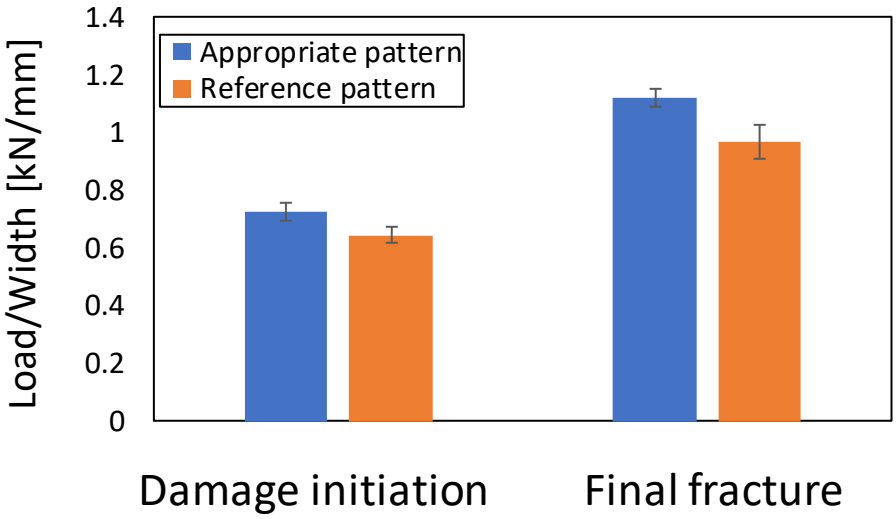
1.4
1.2
1
0.8
0.6
0.4
0.2
0
Load/Width [kN/mm]
Appropriate pattern
Reference pattern
Damage initiation
Final fracture

Fig. 10

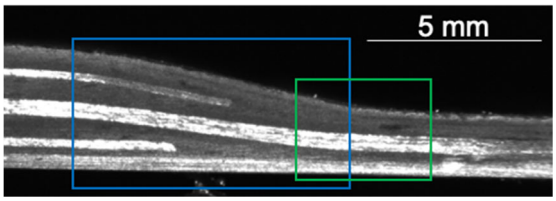

(a)

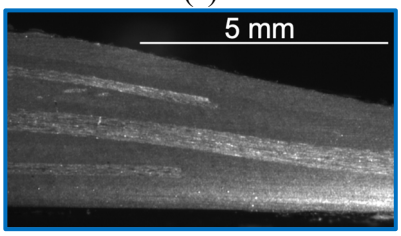

(b)

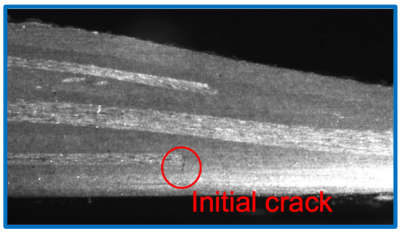

(c)

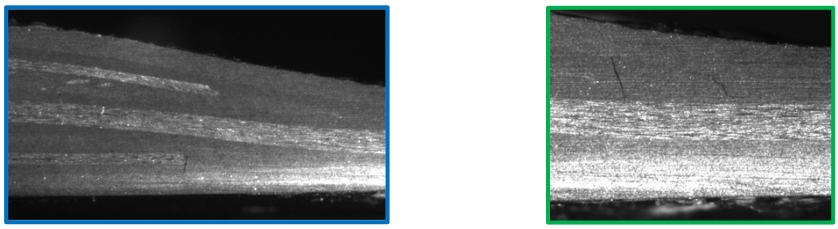

(d)

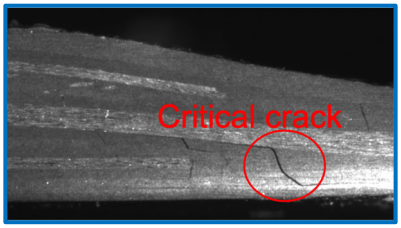

(e)

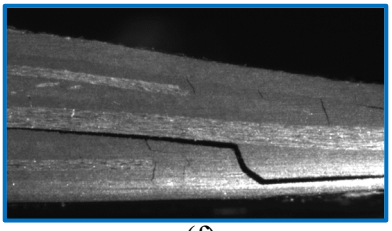

(f)

Fig. 11

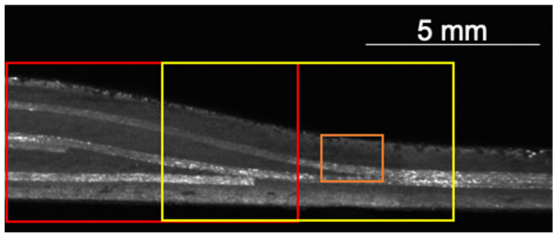

(a)

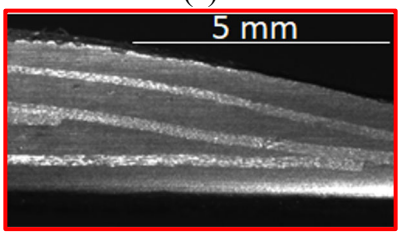

(b)

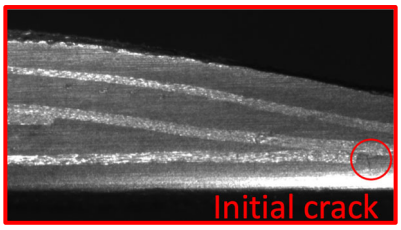

(c)

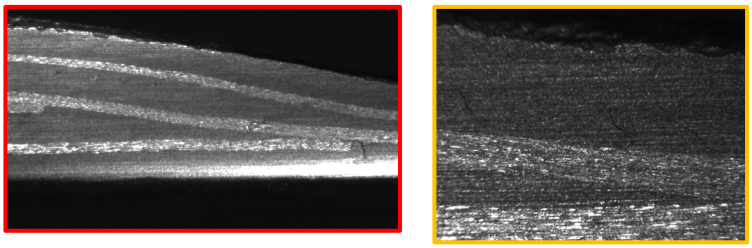

(d)

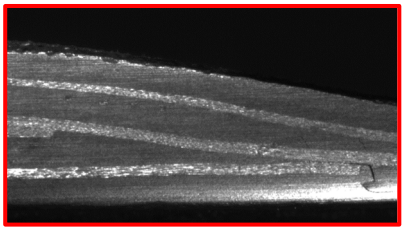

(e)

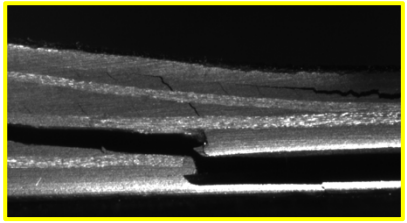

(f)

Fig. 12